Investigating the enhanced photocatalytic degradation of bromophenol blue using Ni/Zn co-doped Strontium Oxide nanoparticles synthesized via hydrothermal method

Shahid Zaman[1], Muhammad Kashif[1], Muffarih Shah[1], Abdul Hameed[1], Noor Majeed[1], Muhammad Ismail[1], Ilyas Khan[1], Saif Ullah[1] & Naqash Khan[2]

[1] Department of Chemistry, Abdul Wali Khan University, Mardan, KP, Pakistan

[2] Department of Biology, University of Haripur, Haripur, KP, Pakistan

Correspondence: Muffarih Shah, Department of Chemistry, Abdul Wali Khan University, Mardan, KP, Pakistan. E-mail: muffarihshah@gmail.com

Received: July 26, 2023 DOI: 10.14295/bjs.v3i1.460

Accepted: August 17, 2023 URL: https://doi.org/10.14295/bjs.v3i1.460

Abstract

Excessive exposure of human to organic contaminants from industrial effluents calls for the implementation of effective pollutants removal techniques. This article investigates the photocatalytic degradation of bromophenol blue dye using Strontium oxide nanoparticles co-doped with Nickel and Zinc. Hydrothermal synthesis produced the nanoparticles, which were subsequently characterized using various analytical techniques. UV/Visible revealed absorption peaks at 294 nm, 306 nm, 311 nm, and 318 nm, while FTIR spectroscopy identified stretching peaks at 416 cm^{-1}, 588 cm^{-1}, and 856 cm^{-1} for Ni-O and Sr-O bonds. The nanoparticles displayed diameters ranging from 30.50 nm to 36.97 nm. EDX analysis confirmed the elemental composition, with Sr and O comprising of approximately 82.02 %, and Ni and Zn approximately 3.21%. Photocatalytic degradation experiments demonstrated that SrO nanoparticles 85.42% degradation efficiency, while co-doped SrO nanoparticles achieved an impressive 97.97% degradation efficiency. This work highlights the potential co-doped SrO nanoparticles as a promising solution for the efficient removal of organic pollutants from the industrial wastewater, addressing environment contamination concerns.

Keywords: Ni and Zn co-doped Strontium oxide, hydrothermal method, nanoparticles, photocatalytic degradation and bromophenol blue.

Investigando a degradação fotocatalítica aprimorada do azul de bromofenol usando nanopartículas de óxido de Estrôncio co-dopadas com Ni/Zn sintetizadas pelo método hidrotérmico

Resumo

A exposição excessiva de humanos a contaminantes orgânicos de efluentes industriais exige a implementação de técnicas eficazes de remoção de poluentes. Este artigo investiga a degradação fotocatalítica do corante azul de bromofenol usando nanopartículas de óxido de Estrôncio co-dopadas com Níquel e Zinco. A síntese hidrotérmica produziu as nanopartículas, que foram posteriormente caracterizadas usando várias técnicas analíticas. UV/Visível revelou picos de absorção em 294 nm, 306 nm, 311 nm e 318 nm, enquanto a espectroscopia FTIR identificou picos de alongamento em 416 cm^{-1}, 588 cm^{-1} e 856 cm^{-1} para Ni-O e Sr-O títulos. As nanopartículas apresentaram diâmetros variando de 30,50 nm a 36,97 nm. A análise EDX confirmou a composição elementar, com Sr e O compreendendo aproximadamente 82,02%, e Ni e Zn aproximadamente 3,21%. Experimentos de degradação fotocatalítica demonstraram que as nanopartículas de SrO apresentam 85,42% de eficiência de degradação, enquanto as nanopartículas de SrO co-dopadas alcançaram uma impressionante eficiência de degradação de 97,97%. Este trabalho destaca os potenciais nanopartículas de SrO co-dopadas como uma solução promissora para a remoção eficiente de poluentes orgânicos de águas residuais industriais, abordando as preocupações de contaminação do meio ambiente.

Palavras-chave: Ni e Zn co-dopados óxido de Estrôncio, método hidrotérmico, nanopartículas, degradação fotocatalítica e azul de bromofenol.

1. Introduction

Dyes are of utmost importance in several sectors of the dyeing and textile industries. More than 100,000 commercially accessible synthetic dyes are commonly utilised in various industries. The dyes commonly utilised are typically obtained from two primary sources, namely coal tar and petroleum intermediates. The combined annual production of these dyes exceeds 7×10^5 tons (Sahu; Singh, 2019, Robinson et al., 2001). Each year, approximately 15% (equivalent to one thousand tons) of non-biodegradable textile dyes are released into natural streams and aquatic bodies via textile waste effluents (Javaid et al., 2021).

In the dyeing and finishing factories, it is customary for approximately 120-280 liters of water to be consumed per kilogram of cloth during the processing phase. Dyes are frequently the first chemical to be acknowledged in industrial waste-water because of their visibility even in a minute quantity (<1 ppm) (Chakraborty et al., 2022). In addition to their adverse physical properties and poisonous character, the escalating output of dyes resulting from the rapid growth of industrialisation has necessitated the development of efficient treatment methods. Hence, several technologies have been examined to mitigate the significant and complex pollutants, with the aim of minimising their detrimental effects on the environment.

Various conventional physical approaches, including activated carbon adsorption, reverse osmosis, and, have been employed for the purpose of dye removal (Tansakul et al., 2011, Oyarce et al., 2021). Nevertheless, these mechanisms just facilitate the movement of pollutants from one medium to another, hence resulting in the occurrence of secondary contamination. Typically, additional measures are necessary for the treatment of solid wastes and renewal of the adsorbent, resulting in an increased financial burden on the whole process. Various chemical processes, including are frequently employed for the purpose of removing synthetic dyes (Epold et al., 2012, Arslan et al., 2000). Nevertheless, the production of toxic and unstable metabolites during these processes has detrimental impacts on the health of both animals and humans.

In recent times, there has been a notable surge in the interest surrounding the utilisation of ZnO nanoparticles in the field of photocatalysis(Sakthivel et al., 2003, Jadhav et al., 2014). This heightened attention can be attributed to the remarkable catalytic activity and quantum efficiency exhibited by ZnO nanostructures, particularly when compared to the extensively employed TiO_2 nanomaterials (Sun et al., 2008). To date, a range of ZnO nanostructures have been employed for the purpose of catalysing the degradation of noxious dyes into less dangerous chemical compounds by the process of photocatalysis under the influence of UV light irradiation. Sun et al. and Kuo et al. conducted experiments to investigate the photo-catalytic degradation of methylene blue and rhodamine-B using ZnO nanobelts and ZnO nanowires on a silicon wafer with the support of SnO2/Sn, respectively.

The results showed that methylene blue was degraded by approximately 94% after 5 hours, while rhodamine-B was degraded by approximately 94% within 300 minutes under UV light illumination(Wang et al., 2009, Sun et al., 2008). In recent times, there has been an increasing use of metal oxides-based materials, such as ZnO (Zada et al., 2022), V_2O_5 (Jenifer et al., 2021), CuO (Sasikala et al., 2016), TiO_2 (Al-Mamun et al., 2022), WO_3 (Verma et al., 2020), Fe_2O_3 (Subaihi; Naglah, 2022), SnO_2 (Mishra et al., 2022), Al_2O_3 (Anbarasu et al., 2020), ZrO_2(Dawoud et al., 2020) , and others, in the field of photocatalysis. Although titanium dioxide (TiO_2) demonstrated efficacy as a catalyst for the degradation of dye compounds when exposed to UV/Visible light irradiation.

One significant limitation of the TiO_2 catalyst is its relatively high cost, which restricts its widespread implementation in commercial settings. Therefore, the development of a cost-effective catalyst for the elimination of stubborn chemicals with enhanced adsorption, efficient degradation, and outstanding light absorption characteristics was of utmost significance (Ahmad et al., 2022). Hence, ZnO has garnered significant attention as a potential photocatalyst due to its advantageous attributes such as cost-effectiveness, abundance, chemical stability, affordability, non-toxicity, environmental friendliness, extended shelf-life, high electron mobility, and favourable quantum yields (Ahmad et al., 2022).

It should be noted that ZnO has the ability to exist in three distinct phases, specifically hexagonal wurtzite, cubic sphalerite, and cubic rock salt. The hexagonal wurtzite phase, which was observed to be highly stable at room temperature, was characterised by the presence of interpenetrating face-centered cubic (FCC) lattices composed of Zn and O (Prasad; Karthikeyan, 2017). In addition, it has been demonstrated that the ZnO semiconductor exhibits exceptional photocatalytic properties and can be synthesised in a wide range of morphologies such as nanorods, nanobowls, nanospheres, nanofilms, nanoparticles, nanodisks, nanotubes, nanoneedles, nanosheets, nanowires, nanowhiskers, and others (Alam et al., 2021, Saleh, 2019).

The present study focuses on the preparation of Ni and Zn co-doped Strontium oxide by hydrothermal method, their characterizations and using for the photocatalytic degradation of Bromophenol Blue dye which is present in various industrial effluent wastes.

2. Materials and Methods

2.1 Chemicals and equipments

Nickel Nitrate and Stronsium Nitrate were purchased from Daejung, S. Korea. Zinc Nitrate, Sodium Hydroxide ang Dye were purchased from Sigm-Aldrich, Schnelldorf, Germany. 10 mL Teflon lined autoclave (Model: Tob new energy, Item No: Tob reactor, China) made of stainless steel with operating temperature utpo 240 °C, Microwave oven (Dawlance Microwave Oven - MD4 N, Output Power 1000W) and Muffle furnace (temperature upto 1300 °C, made by Across International) were used for heating, drying and calcination of samples.

2.2 Synthesis

The synthesis of Strontium oxide nanoparticles was conducted using a hydrothermal method (Figure 1). A solution was prepared by dissolving 4 g of Strontium nitrate hexahydrate in 60 mL of water, which was afterwards stirred. Simultaneously, three distinct solutions comprising Nickel nitrate and Zinc nitrate were created and afterwards introduced into three separate solutions of Strontium nitrate hexahydrate. The mixes were continuously agitated at ambient temperature.

The pH of the mixture was maintained at a basic level by gradually adding a sodium hydroxide solution. Following a specific time period, a white precipitate was observed to have been generated. The precipitate was afterwards dissolved again in the solution, which was then transferred to a Teflon autoclave made of stainless steel. The autoclave was placed in a microwave oven and maintained at a temperature of 150 °C for a duration of 10 to 12 h, resulting in the formation of a crystalline precipitate. The precipitate was subsequently extracted from the Teflon autoclave and subjected to a thorough washing process in order to eliminate any contaminants. The precipitate was subsequently subjected to microwave drying at a temperature of 110 °C, followed by calcination at 450 °C for a duration of 1 h. This process resulted in the formation of Strontium oxide, as well as Strontium oxide doped with Nickel and Zinc.

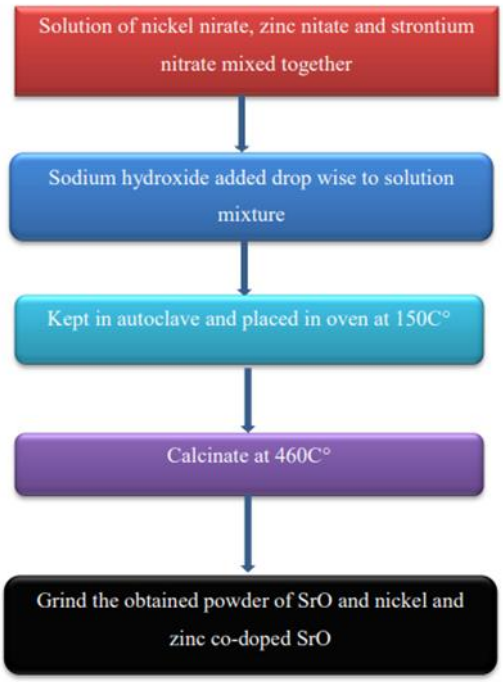

Figure 1. Schematic synthesis of Strontium oxide nanoparticles was conducted using a hydrothermal method.

2.2 Dye degradation

A stock solution of bromophenol blue with a concentration of 10 parts per million (ppm) was generated by dissolving 0.01 g of dry powder dye in 1000 milliliters of distilled water with vigorous agitation. Subsequently, aliquots of working solutions with varying concentrations were extracted from the stock solution and utilised for the purpose of conducting photocatalytic degradation experiments. The dye's photocatalytic degradation was carried out utilising a 100 W incandescent light.

Approximately 0.2 g of photocatalysts were distributed in individual working solutions, which were obtained from a stock solution. These solutions were subsequently left in darkness for a duration of 30 min to allow for the establishment of adsorption/desorption equilibrium prior to the commencement of the photo degradation reaction. Following this, the light bulb was switched on. Various solutions were employed at different time intervals, and the catalysts were subsequently eliminated by the filtration process. The measurement of absorbance for the filtered solution was conducted using a UV-*Vis* spectrometer. The percentage of photodegradation of bromophenol blue was determined by employing the following equation. The degradation percentage can be calculated using the formula:

$$\% \text{ Degradation } = \frac{C_0 - C_t}{C_0} \times 100$$

In this context, the symbol "Co" represents the starting concentration of the dye, while "Ct" represents the concentration of the dye at a given time "t".

2.3 Characterizations

Different characterization methods were entertained to analyze and understand the properties of samples. UV-*Vis* spectroscopic study was conducted using a Shimadzu UV-1800 spectrometer, wavelength range from 190-1100 nm, assisting absorbance measurements. The FT-IR (V. 640, USA) ranges from 400 to 4000 cm^{-1} was used to study functional groups by building spectra from a 0.09 g sample. Photoluminescence (PL) analysis, executed at Abdul Wali Khan University Mardan, played a vital role in evaluating material purity with a spectral range of 230 to 1000 nm and a non-destructive methodology. X-ray diffraction difratometer (D-2 Phaser, Burker, Denver, CO, USA) was used by applying 20 degree per minute, and a Cu kα radiation source was used, providing understandings into the crystalline structure of samples. The shape evaluation of samples was conducted through scanning electron microscope (model, JSM5910, JEOL. Kyoto, Japan) was used with accelarartion voltge of 30 KV was used to analyxe the suface morphology of the samples.

3. Results and Discussion

3.1 UV/Vis specto study

Figure 2 illustrates the UV-Visible spectrum of the samples, with a wavelength range of 230 to 700 mn. The synthesis of the samples is substantiated by the existence of a significant excitonic absorption band at a wavelength of 294 nm. The manufacture of Strontium oxide leads to the creation of monodispersed colloidal particles, which in turn gives rise to the manifestation of quantum size effects (Athar, 2013). The band gap of the Strontium oxide nanoparticles that were synthesised was determined to be approximately 4.21 eV.

The introduction of Zn and Ni as dopants leads to a gradual extension of the absorption edges towards longer wavelength regions. As a consequence, there is a decrease in the band gaps. Interestingly, the absorption edges of SrO nanocrystals doped with various amounts of Ni/Zn co-dopants (namely, 2%, 3%, and 4% of Zn and Ni) occur at roughly 306 nm, 311 nm, and 318 nm, respectively. The Tauc plot was employed to determine the band gaps. The band gaps of Nickel/Zinc-doped Strontium oxide nanocrystals, namely those with 2%, 3%, and 4% nickel/zinc co-doping, have been measured and found to be 4.05 eV, 3.98 eV, and 3.89 eV, respectively. Based on the obtained data, it is evident that the band gap energies of Strontium oxide nanoparticles exhibit a consistent decrease with an increasing quantity of Ni/Zn in the samples.

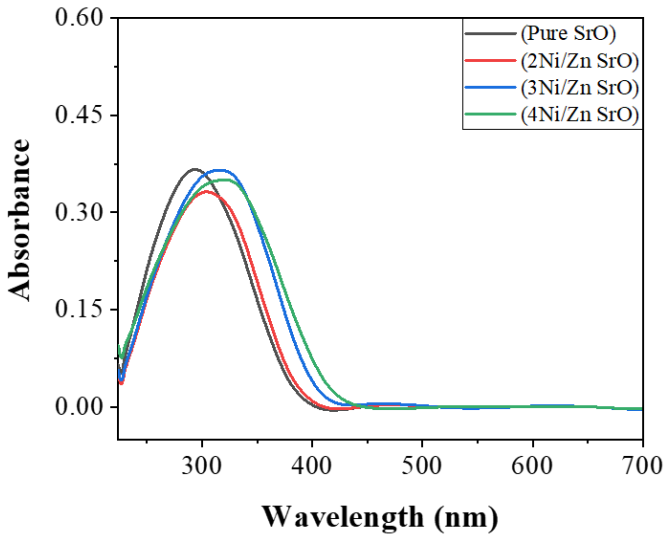

Figure 2. UV-*Vis* spectra of Ni/Zn co-doped Sr-O nanoparticles and pure SrO.

3.2 FT-IR

Figure 3 displays the FTIR spectrum of the synthesised nanostructures. The spectra were collected in the 400 to 4000 cm^{-1} range. Figure 3 depicts the FTIR spectrum of Strontium oxide nanoparticles, which have a band at 705 cm^{-1} and 856 cm^{-1}. Undoped Strontium oxide stretching produced this band. A noticeable peak can be seen in the H-O-H bending at a range of 1452 cm^{-1}. Amino acid C-O stretching occurs in the band at 1033 cm^{-1}. This peak, which ranges from 3000 to 3600 cm^{-1}, demonstrates the presence of both interstitial water molecules and the -OH group. The peak serves as a sign that these two components are present. The apex of the Zn-O and Ni-O stretches, as well as the Ni/Zn-O-H bending vibrations, may arise at around 416 cm^{-1} and 588 cm^{-1}, respectively (Wiercigroch et al., 2017; Akpomie et al., 2022).

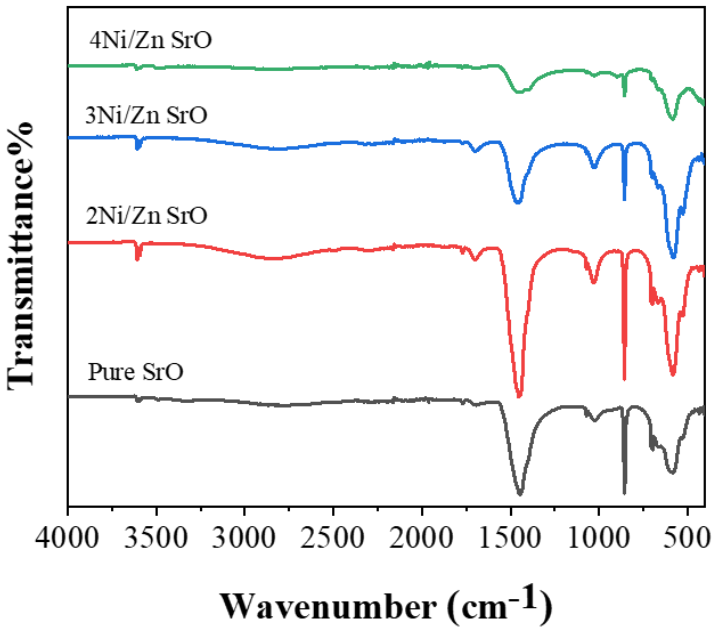

Figure 3. FTIR spectra of Ni/Zn co-doped SrO nanoparticles and pure SrO.

3.3 XRD

Figure displays the XRD information that was obtained from our sample. The crystal planes (101), (200), (310), (211), (111), (301), (200), (210), (510), (411), (600), and (611) of undoped SrO are successively matched to the diffraction peaks at 2-theta = 18.01, 24.76, 30.98, 37.98, 40.93, 42.23, 45.11, 46.33, 48.81, 49.96, and 53.58°.

The samples in question are crystalline materials, as shown by the samples' extremely distinct XRD diffraction peaks. It's fascinating to see that adding Zn and Ni as dopants promotes the growth of the (020), (112), and (114) crystal planes at 14.18, 26.93, and 28.31 degrees while also enhancing the intensity of the XRD peak at 18.01, 24.76, 37.98, and 40.93 degrees. To obtain a precise measurement of the nano-catalyst's crystal size, Scherrer's equation was used.

The average crystallite diameters of 2Ni/Zn SrO, 3Ni/Zn SrO, and 4Ni/Zn Strontium oxide nanoparticles, as well as undoped SrO and Ni/Zn co-doped SrO, are measured in this work. These nanoparticles were measured to have diameters of 30.50, 35.72, 35.81, and 36.97 nm, respectively. The lack of a discernible peak shift in the XRD pattern suggests that the sizes of all the samples are very similar to one another.

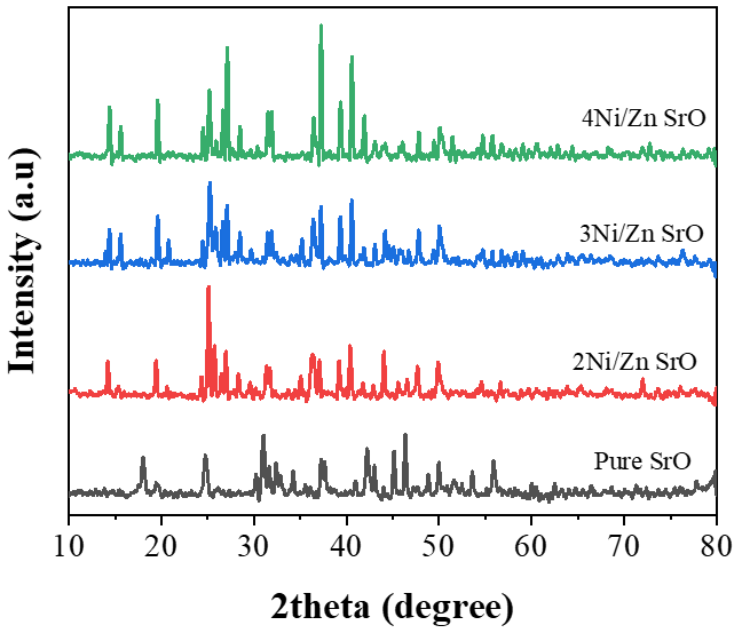

Figure 4. XRD pattern of pure SrO and Ni/Zn co-doped Strontium oxide nanoparticles.

3.4 EDX

Figure 5 displays the EDX results as well as the sample's elemental makeup, which is 2Ni/Zn SrO. The graph demonstrates that zinc, nickel, carbon, and copper have sharp peaks while Strontium and oxygen have high peaks. The samples' exceptional purity is demonstrated by the abundantly obvious inclusion of all required components. Additionally, the sample 2Ni/Zn SrO has considerable amounts of Strontium and oxygen (82.02%), although the amount of doped zinc and nickel is only about 3.21 percent as given EDX table. The final 15% is made up of carbon and copper.

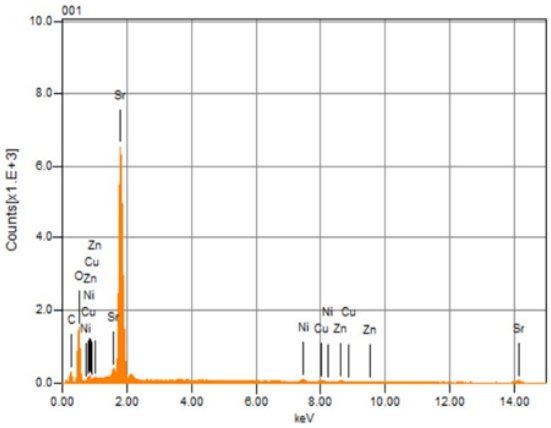

Formula	mass%	Atom%	Sigma	Net	K ratio	Line
C	13.51	30.29	0.04	7445	0.0015752	K
O	30.93	52.07	0.11	38986	0.0376930	K
Ni	1.79	0.82	0.05	5012	0.0071118	K
Cu	1.28	0.54	0.06	3007	0.0049347	K
Zn	1.42	0.58	0.07	2846	0.0055716	K
Sr	51.09	15.70	0.21	361226	0.1951100	L
Total	100.00	100.00				

Figure 5. EDX of the sample.

3.5 PL study

According to the PL spectra, pure Strontium oxide displays peaks that are significantly more intense than those of the other co-doped SrO at 427, 446, 467 nm, 512, and 570 nm. Since PL intensity is a direct indicator of electron-hole recombination, the fact that pure SrO displays a peak that is more intense than that of other samples shows that it undergoes electron-hole recombination often. Because the amount of charge carriers produced by photons directly affects the photocatalytic activity of semiconductors (Martha et al., 2012, Mukherji et al., 2011), pure SrO exhibits less photocatalytic activity. However, all of the Ni/Zn co-doped SrO samples have lower PL intensities when compared to pure SrO. The 3Ni/Zn SrO sample is determined to have the lowest PL intensity. Due to the low PL intensity, it seems as though more excited electrons are trapped and are stably transmitting over the contact (Shah et al., 2013). As a consequence, there is hardly any charge carrier recombination in the case of 3Ni/Zn SrO, which is proof of the materials' improved photocatalytic activity.

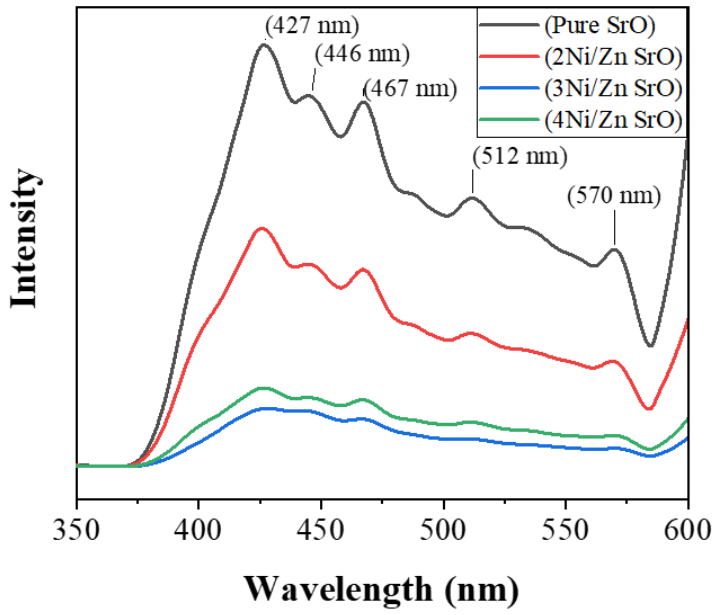

Figure 6. PL spectra of pure SrO and Ni/Zn co-doped SrO NPs.

3.6 Photocatalytic activity

The photocatalytic activity of the produced photocatalysts was investigated while BPB was utilised as a model dye under visible light irradiation in an aqueous medium. Figure 7 shows the UV-vis absorbance spectra of bromophenol blue in an aqueous solution before and after the material was exposed to UV light for intervals ranging from 0 to 210 minutes. To achieve equilibrium between the adsorption and desorption of the dye molecules, the mixture was magnetically stirred for 30 min while left in the dark. At a distance of 7 centimeters from the material being studied, the combination was exposed to visible light generated by a Tungsten filament lamp. At regular intervals of 30 minutes apart, 10 mL aliquots were taken while the reaction mixture was continually stirred. The findings are presented in figure7 after the mixture was centrifuged for five minutes at a speed of 3000 rpm.

The results showed that as the irradiation duration grew from 0 to 210 min, the absorbance of the BPB solution at its maximum wavelength of 591 nm rapidly dropped. The experiment was conducted with this tendency in mind. This shows that bromophenol blue's photodegradation is time-dependent and that it increases with longer exposure to light. The results show that each photo catalyst has outstanding photocatalytic activity against bromophenol blue in the aqueous medium. In the present study, photocatalysts made of pure SrO and Ni/Zn co-doped SrO are responsible for the photocatalytic degradation of bromophenol blue in the aqueous medium. The degradation efficiency of bromophenol blue was found to be best in the case of 3Ni/Zn SrO (97.97%), followed by 2Ni/Zn SrO (95.32%), 4Ni/Zn SrO (93.45%), and pure SrO (85.43%) after 120, 150, 180, and 210 min of irradiation.

It certainly shouldn't come as much of a surprise to hear that the catalytic activity of un-doped Strontium oxide is on the lower side of the spectrum given the large band gap and speedy charge recombination that this chemical features. However, when Ni/Zn is used as a dopant, there is a significant rise in the photocatalytic activity. The quantity of Ni/Zn dopant added also affects how well the photocatalytic degradation works, and the material made of 3Ni/Zn SrO has the maximum degradation effectiveness. However, when the Ni/Zn ratio is increased even further (4 Ni/Zn SrO), the photocatalytic activity is decreased. This is as a result of the shadow effect caused by Ni/Zn. Ni/Zn seems to have a significant role in extending the light absorption and reducing charge recombination in Strontium oxide NPs, as shown by the photocatalytic destruction of BPB. The percentage of deterioration was calculated using the equation below.

$$\text{Degradation efficiency (\%)} = \text{Ao-C/Ao} \times 100\%$$

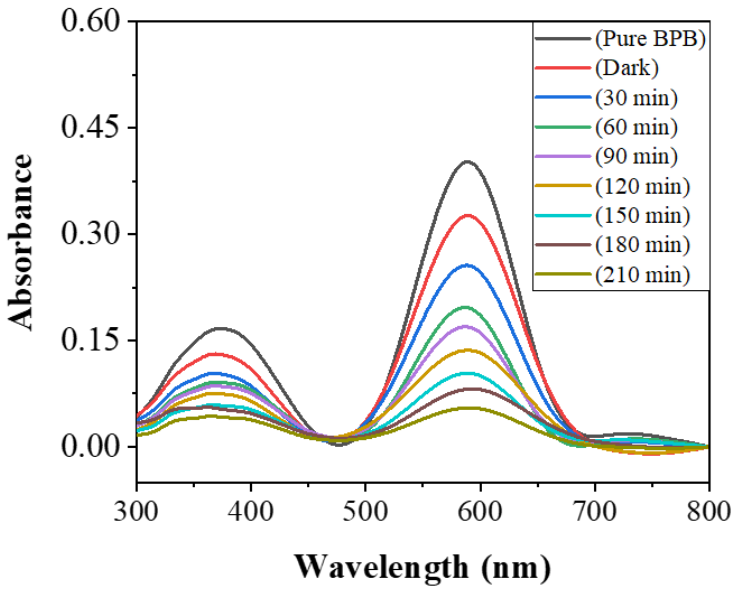

Figure 7. (i) Photocatalytic degradation of BPB utilizing pure Strontium oxide nanoparticles.

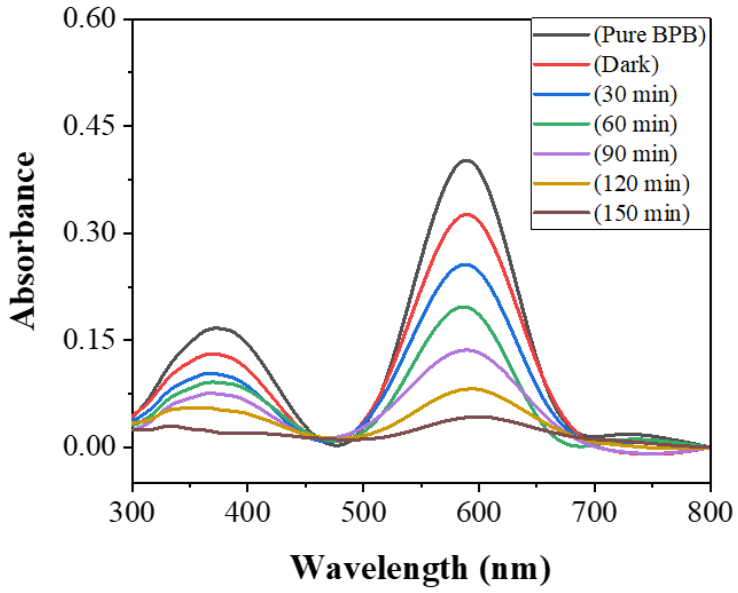

Figure 8. (ii) Photocatalytic degradation of BPB utilizing 2 Ni/Zn co-doped Strontium nanoparticles.

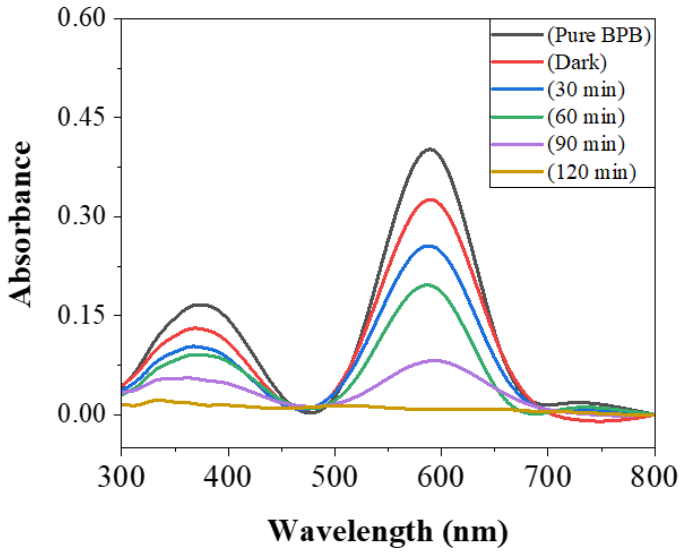

Figure 9. (iii) Photocatalytic degradation of BPB utilizing 3 Ni/Zn co-doped Strontium nanoparticles.

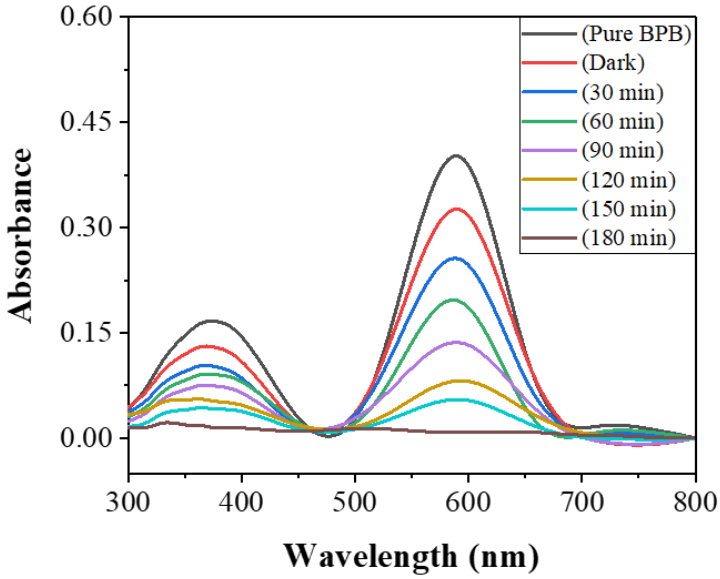

Figure 10. (iv) Photocatalytic degradation of BPB using 4Ni/Zn co-doped Strontium nanoparticles.

Table 1. Time and percent degradations shown by the samples.

Time	**Percent degradation**			
(min)	**Pure SrO**	**2Ni/Zn SrO**	**3Ni/Zn SrO**	**4Ni/Zn SrO**
0	5.9	21.29	25.59	19.85
30	35.31	39.31	41.19	37.11
60	50.24	54.43	62.13	52.23
90	56.96	68.96	81.69	66.05
120	65.16	82.16	97.97	80.89
150	73.37	95.32	-------	87.34
180	78.65	-------	-------	93.45
210	85.34	-------	-------	--------

Note: Pure SrO means pure Stronsium oxide, 2Ni/Zn SrO means 2% Ni and Zn doped Stronsium oxide, 3% 3Ni/Zn SrO Ni and Zn doped Stronsium oxide, and 4Ni/Zn SrO means 4% Ni and Zn doped Stronsium oxide.

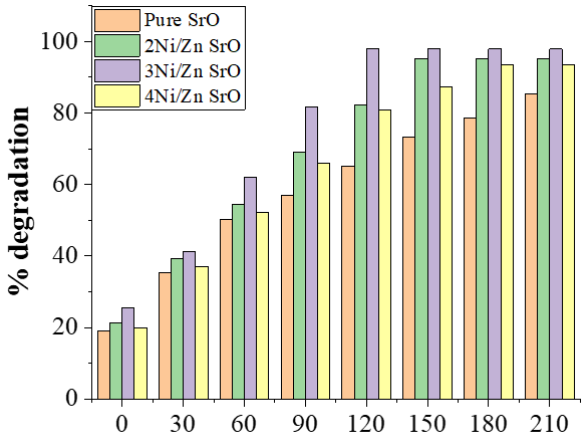

Figure 11. (%) photocatalytic degradation of SrO and 2, 3, 4Ni/Zn doped Strontium oxide NPs.

4. Conclusions

Using the hydrothermal technique, SrO and Ni/Zn co-doped SrO nanoparticles were successfully produced. As-synthesized samples were put through a number of tests, including UV-Vis, FTIR, XRD, SEM, PL, and EDX spectroscopy, to determine form, optical properties, and phase purity. The XRD analysis amply demonstrated the crystalline character of the generated systems.

The modes of vibration present in Strontium oxide deposits were identified using FTIR spectroscopy. We were able to examine the optical properties of Strontium oxide and Ni/Zn co-doped Strontium oxide using UV-vis spectroscopy. Bromophenol blue removal from water using Strontium and Ni/Zn co-doped Strontium oxide photo-catalysts was studied. Strontium oxide nanoparticles only destroyed about 85% of the BPB dye, whereas Ni/Zn co-doped Sr-O photo catalysts degraded more than 97% of it.

5. Acknowledgments

The author is greatly acknowledging the Department of Chemistry, Abdul wali khan university Mardan and University of Haripur, Haripur, Khyber Pakhtunkhwa, Pakistan for providing experimental facilities.

6. Authors' Contributions

Shahid Zaman: conceptualization, methodology, and writing - original draft preparation. *Muhammad Kashif*: investigation, data curation, and formal analysis. *Muffirah Shah*: synthesis of Ni/Zn co-doped Strontium oxide nanoparticles via hydrothermal method and photocatalysis. *Abdul Hameed*: characterization and analysis of photocatalytic properties. *Noor Majeed*: experimental design and data interpretation. *Muhammad Ismail*: supervision, funding acquisition, and project administration. *Ilyas Khan*: manuscript review and editing, contribution to theoretical insights. *Saif Ullah*: validation of results and statistical analysis. *Naqash Khan*: literature review, background research, and manuscript review. All authors have read and approved the final manuscript.

7. Conflicts of Interest

No conflicts of interest.

8. Ethics Approval

Not applicable.

9. References

Ahmad, I., Aslam, M., Jabeen, U., Zafar, M. N., Malghani, M. N. K., Alwadai, N., Alshammari, F. H., Almuslem, A. S., & Ullah, Z. (2022). ZnO and Ni-doped ZnO photocatalysts: Synthesis, characterization and improved visible light driven photocatalytic degradation of methylene blue. *Inorganica Chimica Acta*, 543, 121167. https://doi.org/10.1016/j.ica.2022.121167

Akpomie, K. G., Adegoke, K. A., Oyedotun, K. O., Ighalo, J. O., Amaku, J. F., Olisah, C., Adeola, A. O., Iwuozor, K. O., & Conradie, J. (2022). Removal of bromophenol blue dye from water onto biomass, activated carbon, biochar, polymer, nanoparticle, and composite adsorbents. *Biomass Conversion and Biorefinery*, 1-29. https://doi.org/10.1007/s13399-022-03592-w

Alam, M. W., Aamir, M., Farhan, M., Albuhulayqah, M., Ahmad, M. M., Ravikumar, C. R., Kumar, V. G., & Murthy, H. C. A. (2021). Green synthesis of Ni-Cu-Zn based nanosized metal oxides for photocatalytic and sensor applications. *Crystals*, 11(12), 1467. https://doi.org/10.3390/cryst11121467

Al-Mamun, M. R., Hossain, K. T., Mondal, S., Khatun, M. A., Islam, M. S., & Khan, M. Z. H. (2022). Synthesis, characterization, and photocatalytic performance of methyl orange in aqueous TiO_2 suspension under UV and solar light irradiation. *South African Journal of Chemical Engineering*, 40(1), 113-125. https://hdl.handle.net/10520/ejc-chemeng-v40-n1-a10

Anbarasu, S., Ilangovan, S., Usharani, K., Prabhabathi, A., Suganya, M., Balamurugan, S., Kayathiri, C.,

Karthika, M., Nagarethinam, V. S., & Balu, A. R. (2020). Visible light mediated photocatalytic activity of Ni-doped Al_2O_3 nanoparticles. *Surfaces and Interfaces*, 18, 100416. https://doi.org/10.1016/j.surfin.2019.100416

Arslan, I., Balcioğlu, I. A., & Bahnemann, D. W. (2000). Advanced chemical oxidation of reactive dyes in simulated dyehouse effluents by ferrioxalate-Fenton/UV-A and TiO_2/UV-A processes. *Dyes and Pigments*, 47(3), 207-218. https://doi.org/10.1016/S0143-7208(00)00082-6

Athar, T. (2013). Synthesis and characterization of Strontium oxide nanoparticles via wet process. *Materials Focus*, 2(6), 450-453. https://doi.org/10.1166/mat.2013.1121

Chakraborty, R., Vilya, K., Pradhan, M., & Nayak, A. K. (2022). Recent advancement of biomass-derived porous carbon based materials for energy and environmental remediation applications. *Journal of Materials Chemistry A*, 10(13), 6965-7005. https://doi.org/10.1039/D1TA10269A

Dawoud, T. M., Pavitra, V., Ahmad, P., Syed, A., & Nagaraju, G. (2020). Photocatalytic degradation of an organic dye using Ag doped ZrO_2 nanoparticles: Milk powder facilitated eco-friendly synthesis. *Journal of King Saud University-Science*, 32(3), 1872-1878. https://doi.org/10.1016/j.jksus.2020.01.040

Epold, I., Dulova, N., Veressinina, Y., & Trapido, M. (2012). Application of ozonation, UV photolysis, Fenton treatment and other related processes for degradation of ibuprofen and sulfamethoxazole in different aqueous matrices. *Journal of Advanced Oxidation Technologies*, 15(2), 354-364. https://doi.org/10.1515/jaots-2012-0215

Jadhav, A. H., Patil, S. H., Sathaye, S. D., & Patil, K. R. (2014). A facile room temperature synthesis of ZnO nanoflower thin films grown at a solid–liquid interface. *Journal of Materials Science*, 49, 5945-5954. https://doi.org/10.1007/s10853-014-8313-1

Javaid, R., Qazi, U. Y., Ikhlaq, A., & Zahid, M. (2021). Subcritical and supercritical water oxidation for dye decomposition. *Journal of Environmental Management*, 290, 112605. https://doi.org/10.1016/j.jenvman.2021.112605

Jenifer, A., Sastri, M. S., & Sriram, S. (2021). Photocatalytic dye degradation of V2O5 Nanoparticles—An experimental and DFT analysis. *Optik*, 243, 167148. https://doi.org/10.1016/j.ijleo.2021.167148

Martha, S., Reddy, K. H., Biswal, N., & Parida, K. (2012). Facile synthesis of InGaZn mixed oxide nanorods for enhanced hydrogen production under visible light. *Dalton Transactions*, 41(46), 14107-14116. https://doi.org/10.1039/C2DT31949G

Mishra, P. K., Biswal, S., & Sahu, D. (2022). Synthesis and photocatalytic activity of Ni doped SnO_2 nanoparticles for removal of toxic industrial dyes. *Materials Today: Proceedings*, 68(part 1), 80-84. https://doi.org/10.1016/j.matpr.2022.06.104

Mukherji, A., Seger, B., Lu, G. Q. M., & Wang, L. (2011). Nitrogen doped $Sr_2Ta_2O_7$ coupled with graphene sheets as photocatalysts for increased photocatalytic hydrogen production. *ACS Nano*, 5(5), 3483-3492. https://doi.org/10.1021/nn102469e

Oyarce, E., Roa, K., Boulett., A., Sotelo, S., Cantero-López, P., Sánchez, J., Rivas, B. L. (2021). Removal of dyes by polymer-enhanced ultrafiltration: an overview. *Polymers*, 13(19), 3450. https://doi.org/10.3390/polym13193450

Prasad, N., & Karthikeyan, B. (2017). Cu-doping and annealing effect on the optical properties and enhanced photocatalytic activity of ZnO nanoparticles. *Vacuum*, 146, 501-508. https://doi.org/10.1016/j.vacuum.2017.03.028

Robinson, T., McMullan, G., Marchant, R., & Nigam, P. (2001). Remediation of dyes in textile effluent: a critical review on current treatment technologies with a proposed alternative. *Bioresource Technology*, 77(3), 247-255. https://doi.org/10.1016/S0960-8524(00)00080-8

Sahu, O., & Singh, N. (2019). Significance of bioadsorption process on textile industry wastewater. *In*: The Impact and Prospects of Green Chemistry for Textile Technology, 367-416. https://doi.org/10.1016/B978-0-08-102491-1.00013-7

Sakthivel, S., Neppolian, B., Shankar, M. V., Arabindoo, B., Palanichamy. M., & Murugesan, V. (2003). Solar photocatalytic degradation of azo dye: comparison of photocatalytic efficiency of ZnO and TiO_2. *Solar Energy Materials and Solar Cells*, 77(1), 65-82. https://doi.org/10.1016/S0927-0248(02)00255-6

Saleh, S. M. (2019). ZnO nanospheres based simple hydrothermal route for photocatalytic degradation of azo

dye. *Spectrochimica Acta Part A: Molecular and Biomolecular Spectroscopy*, 211, 141-147. https://doi.org/10.1016/j.saa.2018.11.065

Sasikala, R., Karthikeyan, K., Easwaramoorthy, D., Bilal, I. M., & Rani, S. K. (2016). Photocatalytic degradation of trypan blue and methyl orange azo dyes by cerium loaded CuO nanoparticles. *Environmental Nanotechnology, Monitoring & Management*, 6, 45-53. https://doi.org/10.1016/j.enmm.2016.07.001

Shah, M. S. A. S., Zhang, K., Park, A. R., Kim, K. S., Park, N-G., Park, J. H., & Yoo, P. J. (2013). Single-step solvothermal synthesis of mesoporous Ag–TiO 2–reduced graphene oxide ternary composites with enhanced photocatalytic activity. *Nanoscale*, 5(11), 5093-5101. https://doi.org/10.1039/C3NR00579H

Subaihi, A., & Naglah, A. M. (2022). Facile synthesis and characterization of Fe_2O_3 nanoparticles using L-lysine and L-serine for efficient photocatalytic degradation of methylene blue dye. *Arabian Journal of Chemistry*, 15(2), 103613. https://doi.org/10.1016/j.arabjc.2021.103613

Sun, T., Qiu, J., & Liang, C. (2008). Controllable fabrication and photocatalytic activity of ZnO nanobelt arrays. *The Journal of Physical Chemistry C*, 112(3), 715-721. https://doi.org/10.1021/jp710071f

Tansakul, C., Laborie, S., & Cabassud, C. (2011). Adsorption combined with ultrafiltration to remove organic matter from seawater. *Water Research*, 45(19), 6362-6370. https://doi.org/10.1016/j.watres.2011.09.024

Verma, M., Singh, K. P., & Kumar, A. (2020). Reactive magnetron sputtering based synthesis of WO_3 nanoparticles and their use for the photocatalytic degradation of dyes. *Solid State Sciences*, 99, 105847. https://doi.org/10.1016/j.solidstatesciences.2019.02.008

Wang, Z., Huang, B., Dai, Y., Qin, X., Zhang, X., Wang, P., Liu, H., Yu, J. (2009). Highly photocatalytic ZnO/In_2O_3 heteronanostructures synthesized by a coprecipitation method. *The Journal of Physical Chemistry C*, 113(11), 4612-4617. https://doi.org/10.1021/jp8107683

Wiercigroch, E., Szafraniec, E., Czamara, K., Pacia, M. Z., Majzner, K., Kochan, K., Kaczor, A., Baranska, M., & Malek, K. (2017). Raman and infrared spectroscopy of carbohydrates: a review. *Spectrochimica acta part a: Molecular and Biomolecular Spectroscopy*, 185, 317-335. https://doi.org/10.1016/j.saa.2017.05.045

Zada, A., Khan, M., Hussain, Z., Shah, M. I. A., Ateeq, M., Ullah, M., Ali, N., Shaheen, S., Yasmeen, H., Shah, S. N. A., & Dang, A. (2022). Extended visible light driven photocatalytic hydrogen generation by electron induction from g-C_3N_4 nanosheets to ZnO through the proper heterojunction. *Zeitschrift für Physikalische Chemie*, 236(1), 53-66. https://doi.org/10.1515/zpch-2020-1778

Funding

Not applicable.

Intitutional Review Board Statement

Not applicable.

Informed Consent Statement

Not applicable.